



ISSN: 2230-9926

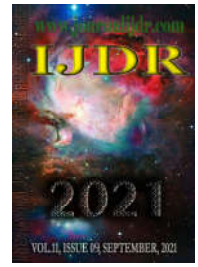
Available online at <http://www.journalijdr.com>

IJDR

International Journal of Development Research

Vol. 11, Issue, 09, pp. 50336-50343, September, 2021

<https://doi.org/10.37118/ijdr.22856.09.2021>



RESEARCH ARTICLE

OPEN ACCESS

COMPACT CIRCULAR POLARIZATION MICROSTRIP FRACTAL ANTENNA DESIGN FOR APPLICATION IN V2X COMMUNICATION IN THE 5.9 GHz BAND

Tales A. C. de Barros*¹, Glaucio F.¹, Paulo H. da F. Silva², Rodrigo C. F. da Silva³ and Elder E. C. de Oliveira⁴

¹Dept. Electrical Engineering, Federal University of Campina Gran, Campina Grande, Brasil; ²Dept. Electrical Engineering, Federal Institute of Paraíba, João Pessoa, Brasil; ³Dept. of Physical, State University of Paraíba, Patos, Brazil; ⁴CBSA Center, State University of Paraíba, João Pessoa, Brazil

ARTICLE INFO

Article History:

Received 08th June, 2021
Received in revised form
11th July, 2021
Accepted 21st August, 2021
Published online 29th September, 2021

Key Words:

Compact Antenna, Circular Polarization, Fractal Microstrip Antenna, Vehicle communication for everything.

*Corresponding author:

Tales A. C. de Barros

ABSTRACT

In this work, the project of a compact circular polarization microstrip fractal antenna for on-board deployment is presented, developed for application in vehicle-to-all communication in the 5.9 GHz operating band. The fractal geometry used as a patch was generated in MATLAB™, from the coded implementation of the Lindenmayer system together with one conformal transformation. To feed the antenna, a proximity transmission line was employed, and to excited two orthogonal modes for circular polarization, a rectangular patch rotated at 45° with a truncated corner was inserted at the end of the transmission line. In addition, to reduce the project's dimensions and operating bandwidth, three antennas were designed with the dielectric substrates: FR-4, RO3006 and RO3010. All antenna design results were analyzed in ANSYS Designer™. Therefore, the microstrip fractal antenna designed with the material RO3010, got at the operating frequency 5.86 GHz, the axial ratio of 0.49 dB, and $|S_{11}|$ of -43.05, directional gain of 6.93 dBi and bandwidth of 255 MHz. The proposed antenna dimension has been reduced by up to approximately 70%, compared to some antennas found in literature. According to the results analyzed and presented, the antenna analyzed is a strong candidate for application in vehicle-to-all communication.

Copyright © 2021, Tales A. C. de Barros et al. This is an open access article distributed under the Creative Commons Attribution License, which permits unrestricted use, distribution, and reproduction in any medium, provided the original work is properly cited.

Citation: Tales A. C. de Barros, 2021. "Compact circular polarization microstrip fractal antenna design for application in v2x communication in the 5.9 ghz band", *International Journal of Development Research*, 11, (09), 50336-50343.

INTRODUCTION

Vehicle-to-vehicle communication (V2V) is not a new technology, the first efforts to standardize this technology date back to 1999 with the FCC (Federal Communication Commission) [1]. The 5.9 GHz frequency spectrum destined by the FCC was used for traffic safety applications such as vehicle collision avoidance (DSRC). With the advancement of wireless communication systems, the standards for communication between vehicles have become more and more stringent, such as IEEE802.11p, which implements, in addition to security, the capability of multiservices through the vehicular network [2]. For communication between vehicles to occur reliably, it is necessary that devices implanted in vehicles have certain requirements such as: reliability in the transmission of information, high data transmission rates, low latency in communication between vehicles and mobility in urban settings with high vehicular density or on roads [3], [4]. As with any other wireless communication network, antennas are the main devices that can provide a secure and fast wireless connection, and can be applied for vehicular communication [5].

As result this, there is a demand created for compact and efficient antennas, for deployment in units on-board OBUs and RSU roads units. Taking into account some characteristics, for communication V2V, microstrip antennas are devices that have inherent advantages over other types of antennas for vehicle deployment or mass manufacturing, such as compact dimensions, easy modeling, the low cost and low profile [6], [7]. On the other hand, microstrip antennas have low directional gain and linear polarization, which can affect the performance of vehicular communication, in mobility and high density scenarios. Therefore, to increase the performance of V2V communication or vehicles and infrastructure, antennas were designed using methods to modify the polarization of the transmit or receive wave or with increase the directional gain, to expand coverage [8] - [13]. In [8], a compact, windshield-shaped antenna was developed with circular polarization for vehicular tracking and location applications. In this project, the circular polarization was generated from the geometric configuration of the antenna patch, and according to the results presented, the axial ratio achieved was equal to 1.81 dB at the central frequency of 1.575 GHz. To increase the signal coverage between V2V communication and satellite communication, an antenna was designed in [9], with two bands of transmission and reception in

the frequencies of 2.60 GHz and 2.98 GHz, in addition to dual circular polarization to the right and to the left, respectively. The geometry of this antenna was projected from a circular patch, and the circular polarization of two directions in the two operating frequencies, generated through two rings projected by L-shaped stumps and suspensions. For applications in ITS (intelligent transport systems), an antenna with multiple resonant frequencies was presented in [10]. According to the results, at the operating frequency at 5.9 GHz, the circular polarization was generated from the implementation of two feeding techniques, coaxial probe and microstrip line, thus, it was possible to observe an axial ratio of less than 3.0 dB in the operating frequency, respectively. In [11], another antenna was proposed for ITS applications, but at the operating frequency of 3.675 GHz. The patch geometry of this antenna was based on the Fern fractal, and according to the results, it was possible to observe a lower axial ratio at 3.0 dB, this result was achieved by fitting a microstrip line network positioned at the bottom of the substrate. For DSRC application at the 5.9 GHz frequency, a high-gain antenna was proposed in [12], this antenna was designed from a circular patch, and to increase the gain, a circular ring and twelve elements in short were inserted around the circular patch. And in [13], another low-profile patch antenna project with psi-shaped geometry was developed for wide bandwidth and circular polarization at the frequency of 5.9 GHz. The circular polarization was generated from the adjustment of dimensions of the patch and the positioning of the transmission line. In this work was developed a microstrip fractal patch antenna Project of polarization circular and compact, from a new fractal geometry, generated in MATLAB™. The method used to generate circular polarization in this project is a patch rotated at 45° with a truncated edge, inserted at the end of the proximity feed line. The present work is divided into the following sessions after the introduction, session II: the work methodology is discussed; in session III, the results of the proposed antenna parameters, generated by the ANSYS Designer™ full wave simulator, are demonstrated; And in session IV conclusions are presented and references are presented in V.

Design of the Antenna

Generation of transformed fractal geometry: The new fractal geometry is generated through a code implemented in MATLAB™. This code performs two functions: first, the Lindenmayer system is executed, to generate the Koch fractal, from the Koch snowflake curve get up the perimeter of a square [14]; the second function is made a transformation conformed according to [15], of type, $w_1 = f(z)$. The complex variable, z , contains the string information (characters conjunct generated by the L-system). Then, after the transformation, $f(z)$, the new fractal geometry can be projected from, w_1 , as illustrated in Fig. 1. Then the image file is exported in Drawing Exchange Format (.DXF) format. to then be imported into the ANSYS Designer™ environment. The analytical equation used in the transformation it was (1):

$$w_1 = f(z) = \cos(z - \frac{\pi}{2}) \quad (1)$$

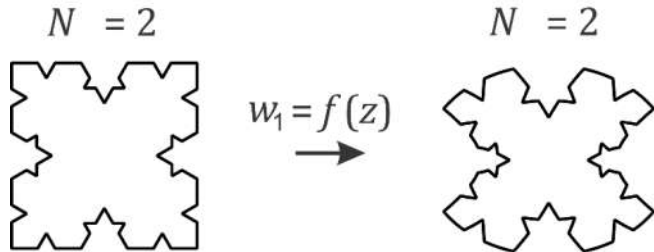


Fig. 1. Conformal transformation of the $N=2$ Koch fractal into a new $N=2$ Koch fractal

Microstrip Fractal Antenna Layout: The microstrip fractal antenna layout is illustrated in Fig. 2. The material used for the initial design was FR-4, whose relative electrical permittivity value, ϵ_r , is equal to 4.4, and the total thickness, h_T , equal to 3.0 mm, take in account the sum of two layers of dielectric substrate with a thickness equal to 1.5 mm, respectively. Antenna dimensions are designed for the resonant

frequency of 5.9 GHz. The dimensions of the fractal patch, W_F and L_F , were approximated to the calculated dimensions of a conventional rectangular patch [7]. For the calculated dimensions, the resonant frequency, f_r , was equal to 5.9 GHz, and the thickness, h_T , equal to 3.0 mm and electrical permittivity equal to 4.4. Comparison of calculated dimensions with dimensions fitted in ANSYS Designer™ are listed in Table I. The dimensions of the transmission line width, W_{LT} , were approximated for an impedance matching of 50.0Ω , [16]. However, the length of the transmission line, L_{LT} , was calculated for a quarter of the guided wave length, $\lambda_g/4$, of the frequency of 5.9 GHz, considering, $\epsilon_r=4.4$. The dimensions of the rotated rectangular patch, W_R and L_R , can define the electrical phase different between the orthogonal modes in 5.9 GHz, necessary for the circular polarization [11], [17]. However, these dimensions excite lower and higher modes, TM_{01} and TM_{21} , respectively, which can affect the resonant frequency at 5.9 GHz as well as the axial ratio. Therefore, the dimensions of the rotated rectangular patch need to be designed for different frequencies than the fractal patch so that they do not overlap at 5.9 GHz.

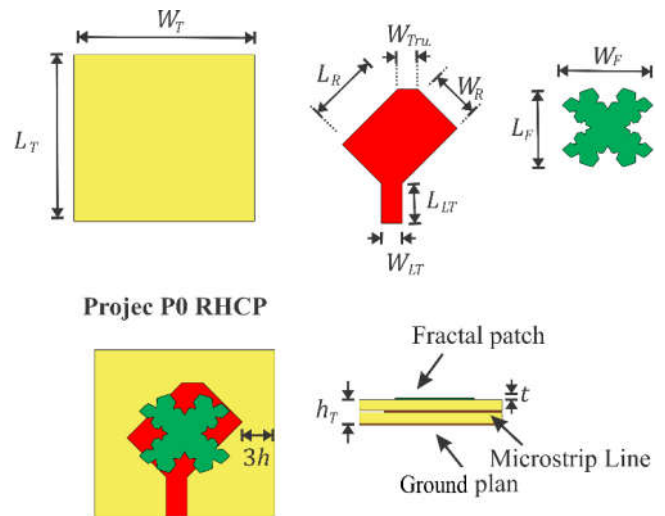


Fig. 2. Layout of the initial circular polarization fractal antenna design

Considering a difference between the frequencies of 1.2 GHz TM_{01} and TM_{21} modes, enough not to overlap with the 5.9 GHz frequency. The frequencies, f_{r1} and f_{r2} , of the TM_{01} and TM_{21} modes, respectively, are given by (2) and (3):

$$f_{r1} = \frac{1.2}{2} - 5.9 = 5.3 \text{ GHz} \quad (2)$$

$$f_{r2} = \frac{1.2}{2} + 5.9 = 6.5 \text{ GHz} \quad (3)$$

With this, the dimension of the length, L_R , is calculated considering, f_{r1} equal to 5.3 GHz, and the width, W_R , considering, f_{r2} equal to 6.5 GHz, initially. In Fig. 3. You can see the comparison graph of the simulation of $|S_{11}|$ of the A0 antenna, designed with the calculated and adjusted dimensions, and the values obtained in Table. II.

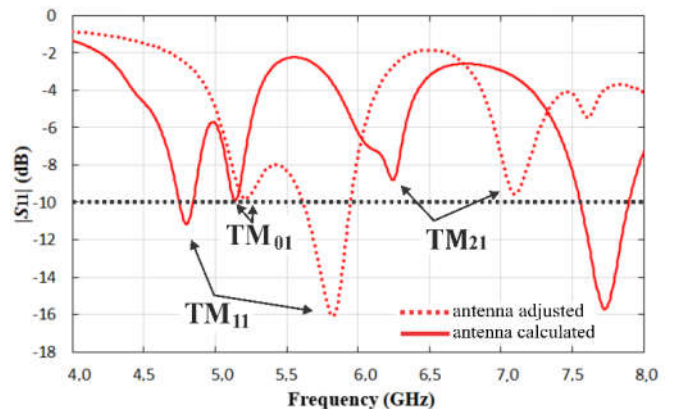


Fig. 3. Simulation of $|S_{11}|$ in dB, in the 4 to 8 GHz range of the adjusted A0 antenna

From the result of the graph, it is observed that the calculated TM_{11} mode frequency of the antenna was 4.79 GHz, which is lower than the frequency for which its dimensions were calculated, that is, 5.9 GHz. This is due to the characteristics of the fractal geometry [14]. Therefore, to increase the TM_{11} mode frequency, the fractal patch dimensions, $W_F \times L_F$, were reduced, and consequently the L_R length, so that the TM_{21} mode frequency does not overlap with the TM_{11} mode frequency.

Table I. A0 antenna dimensions calculated and adjusted in ANSYS Designer™

Dimensions (mm)	Calculated	Adjusted
W_T	26.97	24.81
L_T	25.31	22.93
W_F	15.49	12.40
L_F	10.75	10.73
W_R	9.55	7.60
L_R	11.87	10.70
W_{LT}	2.87	2.87
L_{LT}	5.67	5.49

Table II. Values obtained from the simulation of $|S_{11}|$ of the antenna set A0

Parameters	TM_{01}	TM_{11}	TM_{02}
f_r (GHz), Cal.	5.20	5.82	7.11
f_r (GHz), Adj.	5.14	4.79	6.24
$ S_{11} $ (dB), Cal.	-9.79	-16.07	-9.55
$ S_{11} $ (dB), Adj.	-9.91	-11.15	-8.80
WB (MHz), Cal.	-	330.00	-
WB (MHz), Adj.	-	309.00	-

Table III. A0 antenna dimensions adjusting only LR length

Dimensions (mm)	Adjusted antennas			
	Adj. 1	Adj. 2	Adj. 3	Adj. 4
W_T	24.31	25.07	24.81	25.15
L_T	22.43	22.78	22.93	23.28
W_F	12.40	12.40	12.40	12.40
L_F	10.73	10.73	10.73	10.73
W_R	7.60	7.60	7.60	7.60
L_R	10.00	10.50	10.70	11.20
W_{LT}	2.87	2.87	2.87	2.87
L_{LT}	5.49	5.49	5.49	5.49

Parameter analysis of $|S_{11}|$ and the axial ratio: In this section, the parametric results of the reflection coefficient modulus, $|S_{11}|$, and the axial ratio, AR in dB, of the A0 antenna, with the same FR-4 dielectric substrate with electrical permittivity 4.4 and total thickness 3.0 mm, were analyzed. The first results were obtained by varying only the length of the rotated patch, L_R , as listed in Table III. According to the simulated results of $|S_{11}|$, and illustrated in Fig. 4, it can be seen that the frequency of the TM_{10} mode, f_{r1} , was reduced from 5.30 to 5.14 GHz, with increasing of length, the same occurs with the resonance frequency of the patch fractal, f_r , which varies from 6.02 GHz to 5.73 GHz. Furthermore, it is observed in the frequencies of the TM_{10} and TM_{11} modes, the $|S_{11}|$ less than -17 dB, respectively. For the TM_{21} upper mode, there was little variation compared to the frequencies of the previous modes, as per the values listed in Table IV. The results obtained from the axial ratio in dB, in the frequency range from 5.5 GHz to 6.1 GHz, varying the length, L_R , are illustrated in Fig. 5. As observed, the frequency range with axial ratio below 3.0 dB is reduced, when increases the length, L_R . However, the axial ratio at the center frequency increases and the bandwidth also decreases. The result values are listed in Table V. The simulated results of the $|S_{11}|$ and of A0 antenna axial ratio, adjusting the rotated rectangle patch width, W_R , are presented below. In Table VI, the values used in the variation of width are listed, thus, it can be observed that only the width, W_R , and the dimensions of the ground plane, $W_T \times L_T$, were adjusted according to the previous analysis. The simulated results of $|S_{11}|$ of antenna A0, ranging, W_R , are illustrated in Fig. 6. As seen in the results, the frequency of the top mode, TM_{21} , reduced from 7.31 GHz

to 6.68 GHz with increasing width. Also, when reducing the frequency of TM_{21} mode, the value of $|S_{11}|$ TM_{11} mode frequency is reduced to -36.16 dB. In the TM_{10} mode of frequency there was little variation with the width adjustment, W_R , according to the values listed in Table VII. The simulated results of the axial ratio of the A0 antenna, varying the width, W_R , are compared and illustrated in Fig. 7. As the is increased width, the axial ratio varied from 2.04 dB to 4.26 dB, as well as the frequency of 5.80 GHz up to 5.86 GHz, with the lower axial ratio value. With this in mind, it can be concluded that increasing the width of the rotated rectangular patch can reduce the value of $|S_{11}|$, however, the axial ratio increases for values greater than 3.0 dB, according to the values listed in Table VIII.

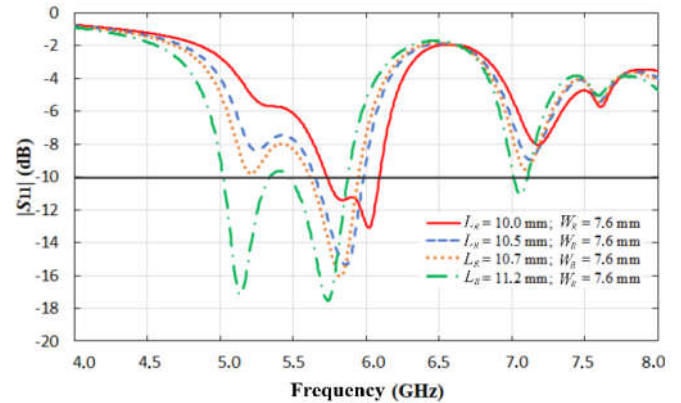


Fig. 4. Simulation of the $|S_{11}|$, of the A0 antenna varying the L_R length

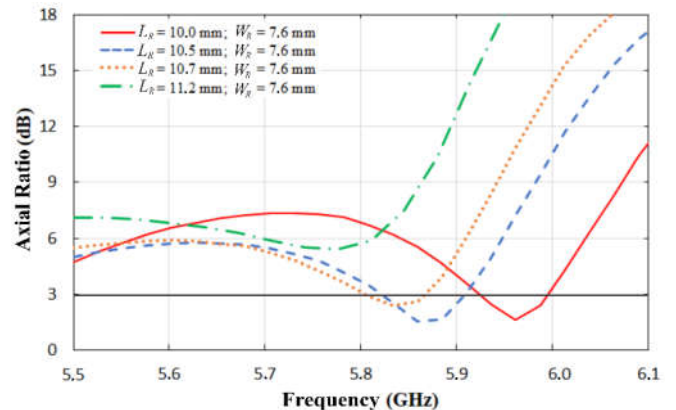


Fig. 5. Axial ratio simulation of antenna A0, varying the L_R length

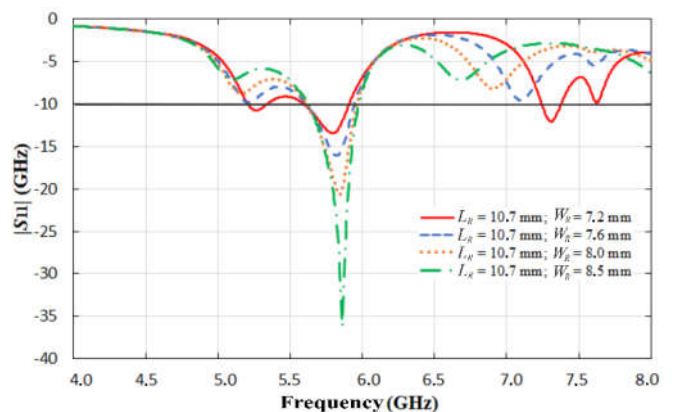


Fig. 6. Simulation of $|S_{11}|$, antenna A0 varying width, W_R

Reduction of project dimensions: The microstrip fractal antennas: A1, A2 and A3, illustrated in Fig. 8, were designed and simulated with the dielectric substrates: FR4, RO3006 and RO3010. The relative electrical permittivity, ϵ_r , of the three dielectric substrates are: 4.4, 6.15 and 10.20, with the following thicknesses, h_T , 3.0 mm, 1.27 mm and 1.27 mm, respectively. Dimensions were calculated and adjusted to optimize resonant parameters as listed in Table IX.

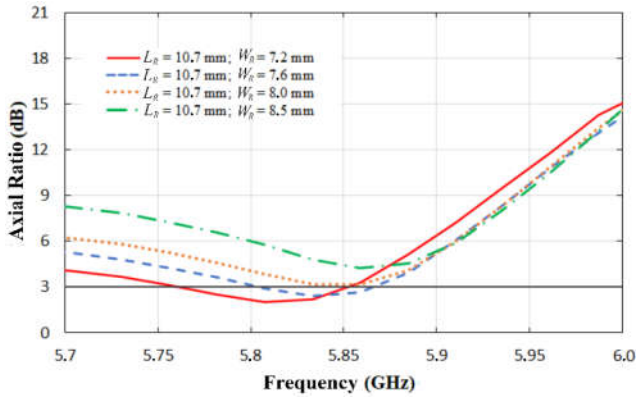


Fig. 7. Axial ratio simulation of antenna A0, varying width, W_R

The objective of this analysis was to reduce the dimensions for a more compact antenna design, and also reduce the bandwidth, WB, in order to reduce the interferences from other applications in frequency bands close to the 5.9 GHz band. Comparison of the simulated results of $|S_{11}|$, in the 5.0 – 7.0 GHz range, of the three antennas A1, A2 and A3, is illustrated in Fig. 9. As expected, the bandwidth of the A3 antenna, designed with RO3010 was 255.0 MHz, much less than the bandwidth of the A1 antenna design with FR4. The result of $|S_{11}|$ of the A3-RO3010 antenna was equal to -43.05 dB at the resonant frequency at 5.88 GHz, indicating an excellent impedance matching in relation to the A1 and A2 antennas, according to the values listed in Table X. The axial ratio simulations of antennas A1, A2 and A3 are compared and illustrated in Fig. 10. According to the results, it is observed that the frequency range with the axial ratio below 3.0 dB was reduced from 101.70 MHz to 50.00 MHz, with an increase in electrical permittivity and the reduction of thickness, between antennas A1 and A3. At the resonance frequency, the axial ratio of the A3 antenna was equal to 0.49 dB, the best result among the three antennas, according to the values listed in Table XI. In the next section, the results of the A3–RO3010 right-circular polarized RHCP antenna with the A3–RO3010 left-circular polarized LHCP antenna are compared and discussed.

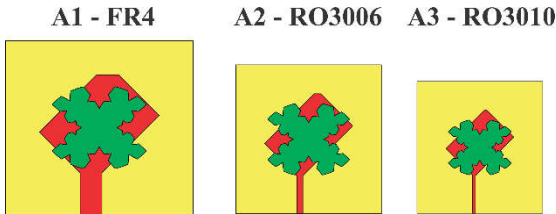


Fig. 8. Comparison of the three simulated antennas with different substrates

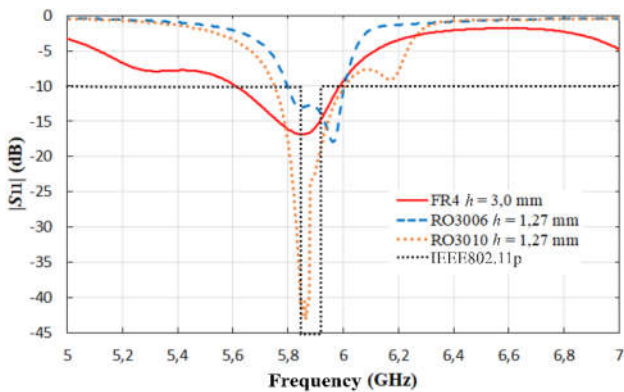


Fig. 9. Comparison of $|S_{11}|$ of antennas A1, A2 and A3

Resultados numéricos da antenna proposta: The two A3–RO3010 antennas, polarized RHCP and LHCP, are designed with the same material, that is, dielectric substrate with, equal to 10.20 and thickness,

h_T , equal to 1.27 mm. The direction of circular polarization is adjusted by changing the rotation direction of the rotated rectangular patch.

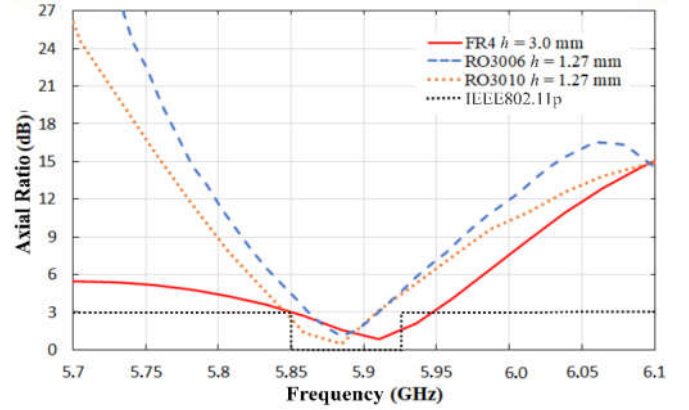


Fig. 10. Comparison of the axial ratio of simulation antennas A1, A2 e A3

In this case, when rotating 45° clockwise, the circular polarization is to the right, and counterclockwise the direction of the circular polarization is to the left, according to the antennas illustrated in Fig. 11.

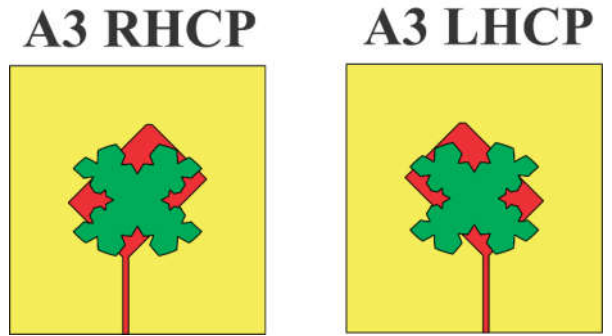


Fig. 11. Two A3 antennas, varying the direction of rotation angle of the rectangular patch

Table IV. Valores obtidos da simulação do $|S_{11}|$ da antenna A0 ajustando o comprimento L_R .

Parameters	Adjusted antennas			
	Adj. 1	Adj. 2	Adj. 3	Adj. 4
f_r (GHz)	6.02	5.86	5.82	5.73
f_{r1} (GHz)	5.30	5.24	5.20	5.14
f_{r2} (GHz)	7.15	7.13	7.11	7.06
$ S_{11} $ (dB)	-13,11	-15.35	-16.07	-17.53
WB(MHz)	355.00	330.00	330.00	395.00

Table V. Values obtained from the simulation of the axial ratio of the antenna a0, varying the length, L_R .

Parameters	Adjusted antennas			
	Adj. 1	Adj. 2	Adj. 3	Adj. 4
f_r (GHz)	5.96	5.88	5.83	5.77
AR (dB)	1.61	1.67	2.38	5.39
WB, CP (MHz)	76.92	88.26	51.28	0.00

Table VI. Values of antenna dimensoes A0 adjusting only the width, W_R .

Dimensions (mm)	Adjusted antennas			
	Adj. 5	Adj. 6	Adj. 7	Adj. 8
W_T	24.31	25.07	24.81	25.15
L_T	22.43	22.78	22.93	23.28
W_F	12.40	12.40	12.40	12.40
L_F	10.73	10.73	10.73	10.73
W_R	7.20	7.60	8.00	8.50
L_R	7.60	7.60	7.60	7.60
W_{LT}	2.87	2.87	2.87	2.87
L_{LT}	5.49	5.49	5.49	5.49

Table VI. Values obtained from the simulation of $|S_{11}|$ of antenna A0 varying width, W_R .

Parameters	Adjusted antennas			
	Adj. 5	Adj. 6	Adj. 7	Adj. 8
(GHz)	5.79	5.82	5.84	5.86
(GHz)	5.27	5.21	5.17	5.14
(GHz)	7.31	7.10	6.91	7.68
(dB)	-13.44	-16.07	-20.63	-36.16
WB (MHz)	315.00	330.00	345.00	335.00

Table VII. Values obtained from the axial ratio of antenna a0, adjusting, W_R .

Parameters	Adjusted antennas			
	Adj. 5	Adj. 6	Adj. 7	Adj. 8
f_r (GHz)	5.80	5.83	5.83	5.86
f_{r1} (GHz)	2.04	2.38	3.17	4.26
f_{r2} (GHz)	102.56	51.28	0.00	0.00

Table VIII. Values obtained from the axial ratio of antenna a0, adjusting, W_R .

Parameters	Adjusted antennas			
	Adj. 5	Adj. 6	Adj. 7	Adj. 8
f_r (GHz)	5.80	5.83	5.83	5.86
AR (dB)	2.04	2.38	3.17	4.26
WB, CP(MHz)	102.56	51.28	0.00	0.00

The simulation comparison of $|S_{11}|$ of the A3 RHCP antenna with the A3 LHCP, is illustrated in Fig. 12. From the result, there is little variation in relation to the resonance frequencies, f_r , of the antennas, being 5.865 GHz for the A3 RHCP antenna and 5.880 GHz for the A3 LHCP antenna. The values of $|S_{11}|$ at the resonant frequencies of antennas were: -43.05 dB and -24.20 dB, respectively. The bandwidth, WB, of the A3 LHCP antenna was 310.0 MHz and was slightly larger than the bandwidth of the A3 RHCP antenna, in this case, equal to 255.0 MHz. The result of the comparison of the axial ratio of the simulated antennas A3 RHCP and A3 LHCP is illustrated in Fig. 13. In this graph, the axial ratio was simulated in the frequency range of 5.7 – 6.1 GHz, with theta, θ , and phi, ϕ , equals to 0° . Thus, the bandwidth of frequencies with AR less than 3.0 dB was 63.50 MHz for the A3 RHCP antenna, and 66.15 MHz for the A3 LHCP antenna. At the antennas' resonance frequencies, the lowest axial ratio values were: 0.49 dB in 5.88 GHz for the A3 RHCP antenna and 1.27 dB in 5.85 GHz for the A3 LHCP antenna, according to the values listed in Table XII.

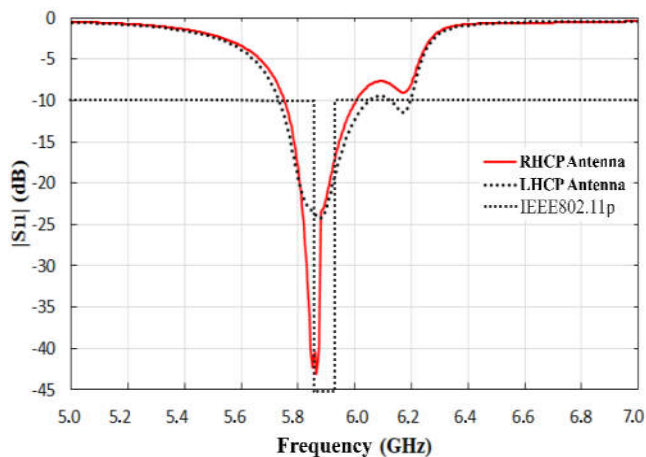


Fig. 12. Values obtained from the simulation of $|S_{11}|$ of the simulated antennas: A3 RHCP and A3 LHCP

The comparison of the axial ratio as a function of theta, considering $\phi = 0^\circ$ and $\phi = 90^\circ$, between the A3 RHCP and A3 LHCP antennas, simulated in 5.865 GHz and 5.880 GHz, respectively, is shown in Fig. 14. In the comparison, the beamwidth of the antennas were approximately 110° with AR less than 3.0 dB, regardless of the Phi variation.

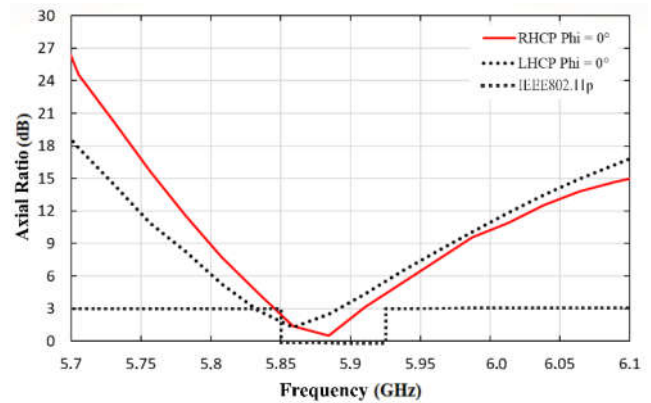


Fig. 13. Comparison of the axial ratio of simulated antennas A3 RHCP and A3 LHCP

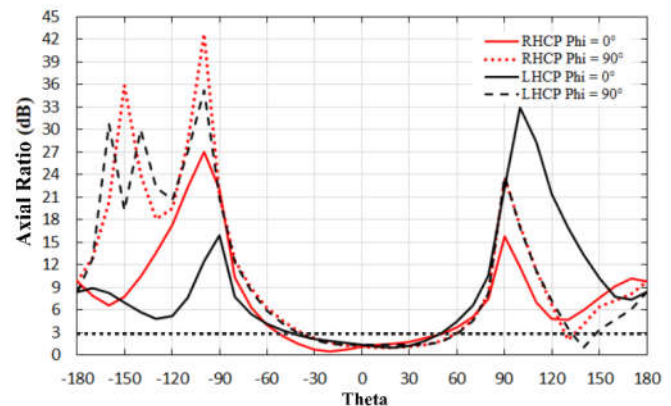


Fig. 14. Comparison of axial ratio versus theta of simulated A3 RHCP and A3 LHCP antennas

In Fig. 15, the radiation diagram of the simulated A3 RHCP antenna at 5.865 GHz is presented. The directional gain obtained in the simulation was 6.389 dBi in the broadside direction, and the half power beamwidth, HPBW, was approximately 111.0° . The result of the simulation of the radiation diagram of the A3 LHCP antenna at the frequency of 5.880 GHz is illustrated in Fig. 16. The directional gain obtained was equal to 6.367 dBi, while the beamwidth, HPBW, was approximately 110.0° , result very close to the A3 RHCP antenna. The surface current density of the A3 RHCP antenna and the far field, simulated at the frequency of 5.865 GHz, are illustrated in Fig. 17. The obtained value was equal to 145.5 A/m^2 . In addition, it is also possible to observe the far field of the antenna, indicating maximum irradiation in the broadside direction.

For the A3 LHCP antenna, the surface current density and the far field were simulated at the frequency of 5.880 GHz, as illustrated in Fig. 18. The value obtained in the simulation of this antenna was equal to 151.58 A/m^2 . For the far field, as well as for the A3 RHCP antenna, maximum irradiation in the broadside direction was indicated. The direction of the right-hand circular polarization of the A3 RHCP antenna can be seen from the rotation of the surface current density as a function of phase, following the right-hand rule, as illustrated in Fig. 19. In addition, it can be observe a 90° phase difference between the components of orthogonal fields in the TM_{11} mode. For the A3 LHCP antenna with left circular polarization direction, the rotation of the surface current density as a function of phase is seen from right to left, following the left hand rule, along the perimeter of the fractal patch, as illustrated in Fig. 20. As seen in the A3 RHCP antenna, the phase difference between the orthogonal fields of the TM_{11} mode is 90° . In Table XIII, the results of the resonant and irradiation parameters of the A3 RHCP antenna were compared with the results of the antennas designed for vehicular communication, found in the literature. For the frequency range of application in vehicular communication systems, the proposed antenna performed better than some of the researched antennas. According to the results presented and discussed, the axial ratio at the central resonance frequency, the

Table VIII. Values of calculated and adjusted dimensions of the three antennas A1, A2 e A3

Dimensions (mm)	A1-FR4		A2-RO3006		A3-RO3010	
	Cal. 1	Adj. 1	Cal. 2	Adj. 2	Cal. 3	Adj. 3
W_T	26.97	24.27	22.00	19.23	18.62	16.58
L_T	25.31	22.78	22.32	19.63	17.95	17.40
W_F	15.49	12.40	13.46	10.82	10.75	8.29
L_F	10.75	10.80	9.91	9.38	7.65	7.22
W_R	9.55	7.60	8.92	6.00	6.87	5.00
L_R	11.87	10.50	10.85	9.30	8.39	7.15
W_{LT}	2.87	2.50	0.40	0.80	0.21	0.37
L_{LT}	5.67	5.49	4.50	5.00	3.35	5.00
h_T	3.00	3.00	1.27	1.27	1.27	1.27

Table IX. Values obtained from the $|S_{11}|$ of the three antennas A1, A2 e A3

Parameters	Antennas A1, A2 e A3		
	Adj. 1	Adj. 2	Adj. 3
f_r (GHz)	5.85	5.96	5.86
f_{r1} (GHz)	5.32	5.84	
f_{r2} (GHz)			6.18
$ S_{11} $ (dB)	-16.85	-17.95	-43.05
WB(MHz)	380.00	210.00	255.00

Table X. Values obtained from the axial ratio of simulated antennas A1, A2 e A3.

Parameters	Antennas A1, A2 e A3		
	Adj. 1	Adj. 2	Adj. 3
f_r (GHz)	5.91	5.88	5.88
AR (dB)	0.87	1.11	0.49
WB, CP (MHz)	101.70	50.00	63.50

Table XI. Values obtained from the axial ratio of simulated antennas A3 RHCP and A3 LHCP

Parameters	A3 RHCP	A3 LHCP
f_r (GHz)	5.88	5.85
AR(dB)	0.49	1.27
WB, CP (MHz)	63.50	66.15

Table XII. Comparison of the parameters of the A3 RO3010 antenna with those of the antenna in the literature

References	f_r (GHz)	$ S_{11} $ (dB)	AR (dB)	Gain (dBi)	WB de AR (MHz)	WB (MHz)
[8]	1.57	-24.90	1.81	-1.20	700.00	400.00
[9]	2.60	-30.00	~3.00	5.76		155.00
[10]	5.91	-42.33	~2.50	4.71		780.00
[11]	3.67	-22.25	~1.50	5.16	90.00	410.00
[12]	5.90	-21.00		1.70		199.00
[13]	5.30	-25.00	0.12	5.00	1000.00	2000.00
Proposed	5.86	-43.05	0.49	6.39	63.50	255.00

Table XIII. Comparison of the parameters of the A3 RO3010 antenna with those of the antenna in the literature

References	$W_T \times L_T$ (mm)	Level	Reduction
[8]	50.00 x 37.00	easy	-84.40
[9]	90.00 x 10.00	difficult	-67.94
[10]	100.00 x 100.00	moderate	-97.11
[11]	30.00 x 30.00	difficult	-67.94
[12]	84.00 x 1.60	difficult	-94.79
[13]	58.20 x 47.70	easy	-89.60
Proposed	16.58 x 17.40	moderate	-

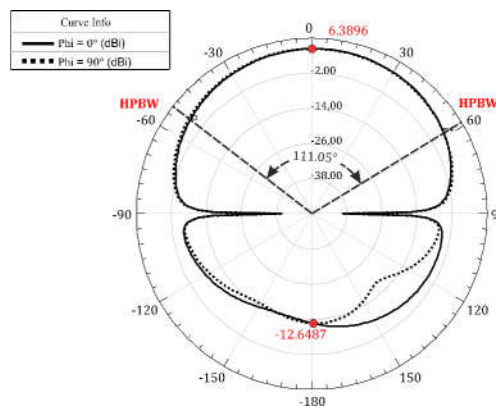


Fig. 15. Simulation of the 2-D radiation diagram at the 5.865 GHz frequency of the RHCP antenna

directional gain and the reflection coefficient modulus, are optimized in comparison with the results of other antennas designed for the same frequency band, as well as for other bands of frequencies intended for application in ITS intelligent transport systems. However, by reducing the transmission bandwidth of the A3 RO3010 antenna to 255.0 MHz, the bandwidth with axial ratio below 3.0 dB was reduced to 63.5 MHz, ie, 9.0 MHz less than the 75.0 MHz band of the standard IEEE802.11p, following the EUA resolution, yet enough for application in C-V2X following the European resolution [4], [18]. Furthermore, the antenna achieved a half-power beamwidth HPBW greater than 100° and good axial ratio for circular polarization at the resonant frequency at 5.865 GHz, close to the central frequency of the IEEE802.11p application.

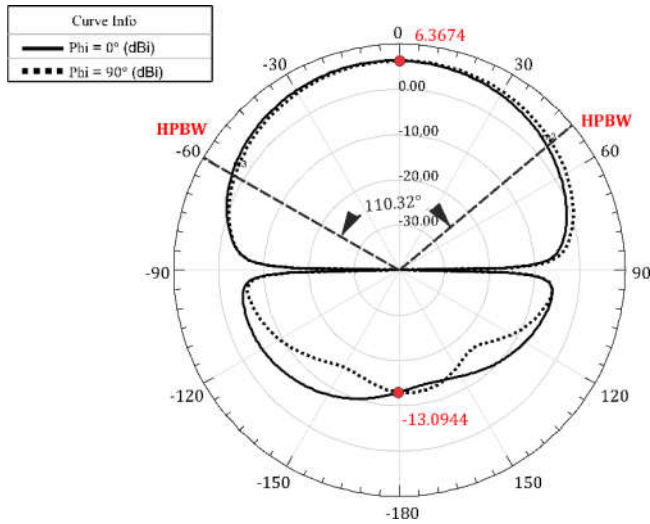


Fig. 16. Simulation of the 2-D radiation diagram at the 5.880 GHz frequency of the LHCP antenna

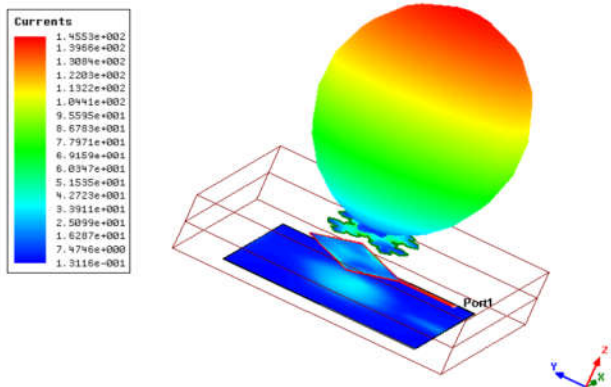


Fig. 17. Simulation of the surface and farfield current density of the A3 RHCP antenna, at the frequency of 5.86 GHz

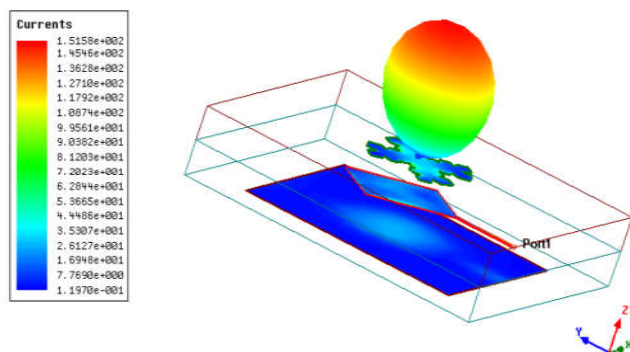


Fig. 18. Simulation of the surface and far field current density of the A3 LHCP antenna, at the frequency of 5.880 GHz

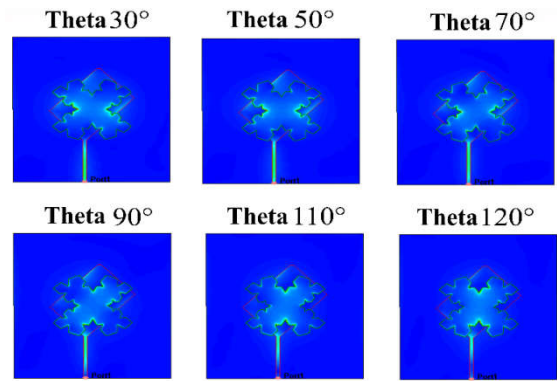


Fig. 19. Surface current variation as a function of the phase of the A3 RHCP antenna

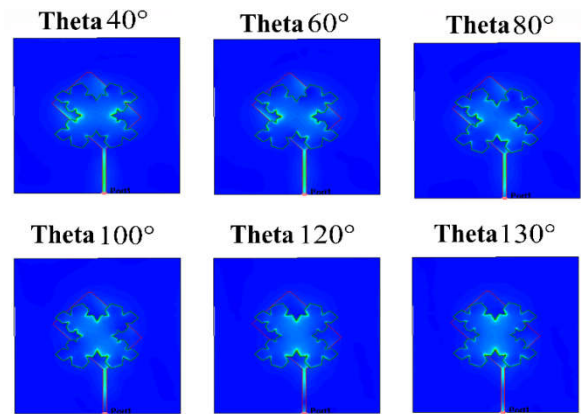


Fig. 20. Surface current variation as a function of the phase of the A3 LHCP antenna

These results together, in addition to ensuring communication in blind spot zones, such as the rear, front or side of any vehicle, combine with another advantage of circular polarization antennas, which in mobility scenarios, the TX and RX antennas do not need to adjust their positions around their propagation axes. In Table XIV, the dimensions and level of complexity of the proposed antenna prototype are listed and compared with some antennas found in the literature. In the table, the percentage reductions of the total area of the proposed antenna in relation to the total area of the researched antennas were also listed and compared. Thus, it can be concluded that the proposed antenna has an area reduction of 97.11%, in relation to the area of the antenna presented in [10], considering that this antenna was designed for a lower frequency range, it could also observe the same manufacturing level. For antennas designed for the same frequency range [9], [11], the proposed antenna presented an area reduction of up to 67.94%. Therefore, the proposed A3 RHCP antenna is more compact than some antennas found in the literature, and can be implemented on vehicle surfaces or embedded without taking up much space.

CONCLUSIO

This document presents a design of a compact circular polarization microstrip fractal antenna, for on-board deployment in vehicles for application in vehicular communication in the 5.9 GHz band. The microstrip antenna was developed from a new fractal geometry, generated from two functions, the L-system together with a conformal transformation, and implemented in MATLAB™ codes. To generate right or left direction circular polarization (RHCP/LHCP), a rectangular patch rotated at 45° with a truncated upper corner was inserted at the end of the proximity microstrip line. According to the results obtained and discussed, the axial ratio, a parameter adopted to measure the polarization of the antenna, was adjusted from the dimensions of the rotated patch, as well as the rotation direction of the circular polarization. In addition, three antenna models were designed

by varying the dielectric substrate to reduce dimensions and bandwidth to reduce interference effects. After reducing the projected antenna bandwidth, the polarization direction was changed to LHCP, adjusting the rotational patch positioning angle. The results of the resonant parameters of the LHCP antenna were compared with those of the RHCP antenna and little variation was observed with the change in the circular polarization direction. Therefore, the antenna presented in this research is suitable for wireless vehicular communication, regardless of the direction of circular wave polarization for communication links: V2V, V2I, V2P, or other links such as satellite communication. The antenna dimensions are compact in relation to the dimensions of other antennas found in the literature, and its manufacture is moderate, being able to be manufactured on a large scale.

ACKNOWLEDGEMENTS

We thank Coordination for the Improvement of Higher Education Personnel (CAPES) for their support finance to this research.

REFERENCES

- Balanis, C. A., *Antenna theory: analysis and design*, 3rd ed. vol 1, John Wiley & Sons, Canada. 1997, pp. 146-154.
- Boban, M., Kousaridas, A., Manolakis, K., Eichinger, J. e W. Xu. "Connected Roads of the Future: Use Cases, Requirements, and Design Considerations for Vehicle-to-Everything Communications," in *IEEE Vehicular Technology Magazine*, vol. 13, não. 3, pp. 110-123, set. 2018, doi: 10.1109 / MVT.2017.2777259.
- Delillo, T. K. The accuracy of numerical conformal mapping methods: a survey of examples and results, *SIAM J. Numer. Anal.* 31 (1994), 788-812.
- ETSI, "Intelligent transport systems (ITS); European profile standard for the physical and medium access control layer of intelligent transport systems operating in the 5G GHz frequency band," European Telecommunications Standards Institute, Sophia Antipolis France, Tech. Rep. ETSI ES 202 663 V1.1.0 (2009-11), 2009.
- ITS Standards. IEEE 1609 - Family of Standards for Wireless Access in Vehicular Environments (WAVE). <<http://www.standards.its.dot.gov/Fctsheets/Factsheet/80>>. Acessado em 23 de março de 2021.
- Kumar, G. and Ray, K. P. *Broadband Microstrip Antennas*, Artech House, Boston, London, 2003. ISBN: 1-58053-244-6.
- Liu, A., Lu, Y., Huang, L. (2018). Low-profile patch antennas with enhanced horizontal omnidirectional gain for DSRC applications. in *IET Microwaves, Antennas & Propagation*, 12(2), 246–253. doi:10.1049/iet-map.2017.0845.
- Liu, G. et al., "Vision, requirements and network architecture of 6G mobile network beyond 2030," in *China Communications*, vol. 17, no. 9, pp. 92-104, Sept. 2020, doi: 10.23919/JCC.2020.09.008.
- Mandelbrot, B., Mandelbrot. *The Fractal Geometry of Nature*. W. H. Freeman and Company, Nova Iorque, 1975.
- Mao, C., Gao, S., and Wang, Y., "Dual-Band Full-Duplex Tx/Rx Antennas for Vehicular Communications," in *IEEE Transactions on Vehicular Technology*, vol. 67, no. 5, pp. 4059-4070, May 2018, doi: 10.1109/TVT.2017.2789250.
- Mondal, T., Maity, S., Ghatak, R., and Chaudhuri, S. R. B. "Compact Circularly Polarized Wide-Beamwidth Fern-Fractal-Shaped Microstrip Antenna for Vehicular Communication," in *IEEE Transactions on Vehicular Technology*, vol. 67, no. 6, pp. 5126-5134, June of 2018, doi: 10.1109/TVT.2018.2824841.
- Mondal, T., Maity, S., Ghatak, R., Chaudhuri, S. R. B., Design and analysis of a wideband circularly polarised perturbed psi-shaped antenna. in *IET Microwaves, Antennas & Propagation*. Vol. 12, Issue 9, 25 July 2018, p. 1582 – 1586. DOI: 10.1049/iet-map.2017.0569.
- Qualcomm. 5G NR Based C-V2X. <<http://www.qualcomm.com/media/docum.ents/fil es/5g-nr-based-c-v2x-presentation.pdf>>. Acessado em 15 de abril de 2021.
- SAB, EF Sundarsingh e HA, "A Compact Conformal Windshield Antenna for Location Tracking on Vehicular Platforms," in *IEEE Transactions on Vehicular Technology*, vol. 68, n° 4, pp. 4047-4050, april of 2019, doi: 10.1109 / TVT.2019.2898709.
- Tales A. C. de Barros, Paulo H. F. Silva, Lamarks T. C. Cavalcanti, Rodrigo C. F. da Silva, Pedro Carlos de Assis Júnior et al. "Broadband patch antennas bio-inspired in the elliptical leaf developed with the riemann transformation for wlan and 5g applications", *International Journal of Development Research*, 10, (06), 36776-36781.
- Upadhyay, G., Kishore, N., RAJ, S., Tripathi, S., & Tripathi., V. A Dual Feed CSRR Loaded Switchable Multiband Microstrip Patch Antenna for ITS Applications. *IET Microwaves, Antennas & Propagation*. doi:10.1049/iet-map.2018.5269.
- Volakis, J. L., Daid, R. J. *Antenna Engineering Handbook – Microstrip Antennas*. University of Houston, McGraw-Hill Companies, 4 ed. 2007.
- Wang, S., Zhu, L., Zhang, G., Yang, J., Wang, J. e Wu, W., " Dual-Band Dual-CP All-Metal Antenna With Large Signal Coverage and High Isolation Over Two Bands for Vehicular Communications," in *IEEE Transactions on Vehicular Technology*, vol. 69, n° 1, pp. 1131-1135, january of 2020, doi: 10.1109 / TVT.2019.2952880.
